

# Commuting Conditional GANs for Robust Multi-Modal Fusion

Siddharth Roheda\*, Hamid Krim\*, and Benjamin S. Riggan†.

\*North Carolina State University at Raleigh, NC, USA

†University of Nebraska-Lincoln, Lincoln, NE, USA

**Abstract**—This paper presents a data driven approach to multi-modal fusion, where optimal features for each sensor are selected from a hidden latent space between the different modalities. The hidden space, as an intrinsic structure, is then exploited in the detection of damaged sensors, and in subsequently safeguarding the performance of the fused sensor system. Experimental results show that such an approach can make the system robust against noisy/damaged sensors, without requiring human intervention to inform the system about the damage.

## I. INTRODUCTION

**I**N recent years, multi-modal fusion has attracted a lot of research interest, both in academia, and in industry. Multi-modal fusion entails the combination of information from a set of different types of sensors. In particular, target detection and recognition problems have widely used a multi-modal approach in order to boost performance. Different sensors may provide different information about a target, and hence, a fusion system combining information from multiple sensors is expected to yield a better performance than that obtained from an individual sensor. Such a fusion of sensor data, however, requires some principled strategy to ensure that additional data is constructively used, and has a positive impact on performance. Sensor fusion is known to broadly classify fusion techniques into three classes. Data level fusion is used when one wishes to combine raw data, and then proceed with inference. Feature level fusion first extracts information from raw data, and then merges these features to make coherent decisions. Finally, the latest point at which one can perform fusion is known as decision level fusion. Fusion at the decision level allows each sensor to reach its own individual decision (on the target identity), prior to an optimal combination of these decisions.

Decision level fusion has received a lot of attention when managing heterogeneous modalities, as it allows each modality to have an independent feature representation, thus providing additional information. A review of classical fusion approaches can be found in [1], [2], and a more recent alternative data-driven perspective is provided by [3]. Over the years, many techniques like Bayesian Fusion [4], and Dempster-Shafer Fusion [5] have been widely used to combine sensor modalities at the decision level. More recently, approaches for fusion have been proposed [6], [7], [8], including for instance, a network of similar and dissimilar sensors. Similar Sensor Fusion [6], [7] is when all sensors explore the same characteristics of the target, while Dissimilar Sensor Fusion [6], [8] is when

different and possibly incompatible sensors observe different characteristics of the target, to hence provide new information about the target. Another fusion framework is presented in [9], [10], to carry out inference by cataloging for each sensor, sets of events, along with their probabilistic characterization, and following a joint probabilistic and thus a coherent evaluation of these events. These events are formalized and associated with each sensor according to its potentially extracted attributes which in turn define given targets. This results in an assignment of a probability measure to each target of interest. The major drawback with this approach is the necessity of hand-picking the features which are subsequently used to define the target defining events. This makes classification/fusion particularly challenging when the target high level features (eg. velocity, weight, etc.) are unknown.

The viability of many fusion approaches strongly hinges on the functionality of all the sensors, making it a fairly restrictive solution. The severity of this limitation is even more pronounced in unconstrained surveillance settings where the environmental conditions have a direct impact on the sensors, and close manual monitoring is difficult or even impractical. Partial sensor failure can hence cause a major drop in performance in a fusion system if timely failure detection is not performed. Furthermore, even if these sensors are successfully detected, the common adopted solution is to ignore the damaged sensor, with a potential negative impact on the overall resulting performance (i.e. relative to when all sensors are functional). We consider exploiting the prior information about the relationship between these sensor modalities, typically available from past observations during training of the fusion system, so that the latter can safeguard a high performance. Recently there has been an interest in such a transfer of knowledge. In [11], the authors introduce hallucination networks to address a missing modality at test time by distilling knowledge into the network during training. Here, a teacher-student network is implemented using an  $L^2$  loss term (hallucination loss) to train the student network. This idea has been further extended in [12], [13], [14]. In [14] where a Conditional Generative Adversarial Network (CGAN) was used to generate representative features for the missing modality. Furthermore, [15] shows that considering interactions between modalities can often lead to a better feature representation. Recent work in Domain Adaptation [16], [17], [18] addresses differences between source and target domains. In these works, the authors attempt to learn intermediate domains (represented as points on the Grassman

manifold in [16], [17] and by dictionaries in [18]) between the source domain and the target domain.

**Our Contributions:** In this paper, we propose a robust sensor fusion algorithm, that can detect damaged sensors on the fly, and take the required steps to safeguard detection performance. We use a special case of the Event Driven Fusion technique recently proposed in [9], [10], and modify it in order to include reliability of individual sensors. This reliability measure is adaptive, and accounts for the sensor condition during implementation. We also propose a data driven approach for learning the features of interest which were handcrafted in [9]. In addition, we learn a hidden latent space between the sensor modalities, and the optimal features for classification are driven by the existence of this hidden space. Furthermore, it also provides robustness against damaged sensors. This hidden space is learned via a generative network conditioned on individual sensor modalities. Unlike [14], we do not require any target feature space in order to learn the optimal hidden space estimates. The hidden space is structured so that it can accommodate both *shared and private* features of sensor modalities. Unlike [10], we do not need to assume a-priori knowledge about sensor damage, and can detect damaged sensors based on deviations in the generated hidden space.

## II. RELATED WORK

### A. Model Based Sensor Fusion

1) *Similar Sensor Fusion:* This model for sensor fusion assumes that independent sensors in the network are similar to each other (eg. 5 radars looking at the same object). Additional sensors in this case do not provide any new information, but can be used to confirm information from other sensors. This model attempts to find a fusion result which is most consistent with all the individual sensor reports. Given a set of objects/targets,  $O = \{o_1, o_2, \dots, o_I\}$ , the  $l^{th}$  sensor report is defined as  $R^l = \{P^l(o_i)\}$ . In order to find the fused report,  $R^f = \{P^f(o_i)\}$ , a cost function is defined such that it measures the discrepancy between the fusion result and each sensor report,

$$R^f = \min_r \sum_{l=1}^L w^l \cdot dist(r, R^l), \quad (1)$$

where,  $w^l$  determines the contribution of the  $l^{th}$  sensor report towards the fused report, and  $dist(A, B)$  is a distance function measuring the discrepancy between the distributions  $A$  and  $B$ . In [6], a Kulback-Liebler distance is used as the distance measure.

2) *Dissimilar Sensor Fusion:* The Dissimilar Sensor Fusion model makes the assumption that all sensors observe dissimilar characteristics of the target, and hence each sensor provides novel information about the target. An additional sensor in this case generates increased resolution on the target identity. The cost function is then formulated so that the solution yields a fusion report representing an enhanced resolution on the target identity, given the individual sensor reports. The optimization

problem to be solved is,

$$\begin{aligned} P^f = \min_p \sum_{l=1}^L w^l \sum_{i=1}^I \frac{1}{P^l(o_i)} p(o_i) - \sum_{i=1}^I \ln(p(o_i)) \\ \text{subject to: } \sum_{i=1}^I p(o_i) = 1, \quad p(o_i) \geq 0. \end{aligned} \quad (2)$$

These two models should be viewed as “extreme cases” of decision level fusion. There are many practical cases in which the sensors are neither completely similar nor completely dissimilar. Event Driven Fusion [9], [10] addresses this limitation and is discussed below.

### B. Event Driven Fusion

Event Driven Fusion looks at fusion under a different light, by combining occurrences of events to reach a probability measure for a target identity. Each sensor is said to make a decision on the occurrence of certain events that it observes, rather than making a decision on the target identity. This technique also explores the extent of dependence between features being observed by the sensors, and hence generates more informed probability distributions over the events.

Consider the set of objects/targets,  $O = \{o_1, o_2, \dots, o_I\}$ . Let the  $k^{th}$  feature from the  $l^{th}$  sensor be  $F_k^l$ . Then, a mutually exclusive set of events,  $\Omega_k^l = \{a_{kj}^l\}_{j=1, \dots, J_{kl}}$ , is defined over the feature  $F_k^l$ . Here,  $a_{kj}^l$  is the  $j^{th}$  event on  $F_k^l$  and is described as  $a_{kj}^l : F_k^l \in [u_j, v_j]$ ,  $u_j \in \mathbb{R}^+$ ,  $v_j \in \mathbb{R}^+$ , and  $v_j > u_j$ . A probability report is generated by the  $l^{th}$  sensor for each of its features,  $R_k^l = \{\Omega_k^l, \sigma_B(\Omega_k^l), P_k^l\}$ . An object/target is then defined as  $o_i \in \sigma_B(\Omega)$ , where,  $\Omega = \Omega_1^1 \times \dots \times \Omega_k^l \times \dots \times \Omega_L^L$ . The joint probability in the product space is determined as a convex combination of a distribution with minimal mutual information and one with maximal mutual information. For events  $\gamma_k^l \in \sigma_B(\Omega_k^l)$

$$\begin{aligned} P_\Omega(\gamma_1^1, \dots, \gamma_k^l, \dots, \gamma_L^L) = \rho \cdot P_{\Omega_{\text{MAXMI}}}(\gamma_1^1, \dots, \gamma_k^l, \dots, \gamma_L^L) + \\ (1 - \rho) \cdot P_{\Omega_{\text{MINMI}}}(\gamma_1^1, \dots, \gamma_k^l, \dots, \gamma_L^L), \end{aligned} \quad (3)$$

where  $\rho \in [0, 1]$  is a pseudo-measure of correlation between the features.  $\rho \approx 1$  when the features are highly correlated, and  $\rho = 0$  when they are independent. For any object defined as a combination of events in the product space  $\Omega$ ,  $o_i \in \sigma_B(\Omega)$ , rules of probability can then be used to determine the object probability. For instance, in a 2-D scenario, an object may be defined as a combination of events  $\gamma_1 \in \sigma_B(\Omega_1)$ , and  $\gamma_2 \in \sigma_B(\Omega_2)$ . The combination defined in the product space,  $\Omega = \Omega_1 \times \Omega_2$ , may be of the form  $o : \{\gamma_1 \wedge \gamma_2\}$  or  $o : \{\gamma_1 \vee \gamma_2\}$ . Given the joint probability,  $P_\Omega$ , rules of probability can be used to determine the fused object probability as follows:

- $o : \{\gamma_1 \wedge \gamma_2\} : P^f(o) = P_\Omega(\gamma_1, \gamma_2)$
- $o : \{\gamma_1 \vee \gamma_2\} : P^f(o) = P_1(\gamma_1) + P_2(\gamma_2) - P_\Omega(\gamma_1, \gamma_2)$

Where,  $P_1(\gamma_1)$  and  $P_2(\gamma_2)$  are the marginal probabilities for detection of the events  $\gamma_1$  and  $\gamma_2$  as seen by sensors 1 and 2.

### C. Generative Adversarial Networks

The Adversarial Network was first introduced by Goodfellow et al. [19] in 2014. In this framework, a generative model

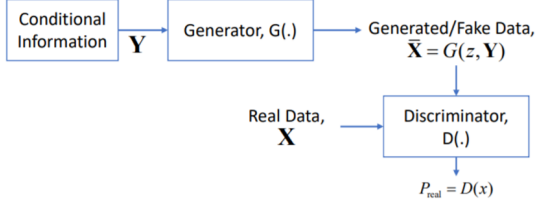


Fig. 1: Conditional Generative Adversarial Networks

is pitted against an adversary: the discriminator. The generator aims to deceive the discriminator by synthesizing realistic samples from some underlying distribution. The discriminator on the other hand attempts to discriminate between a real data sample and that from the generator. Both these models are approximated by neural networks. When trained alternatively, the generator learns to produce random samples from the data distribution which are very close to the real data samples. Following this, Conditional Generative Adversarial Networks (CGANs) were proposed in [20]. These networks were trained to generate realistic samples from a class conditional distribution, by replacing the random noise input to the generator by some useful information (see Figure 1). Hence, the generator now aims to generate realistic data samples, given the conditional information. CGANs have been used to generate random faces, given facial attributes [21] and to also produce relevant images given text descriptions [22].

*Discussion on Conditional Generative Adversarial Networks:* In this section, we explore and uncover some limitations of Conditional Generative Adversarial Networks, when tasked with generating figures with limited support and otherwise. We take a simple example where the input to the network is uniformly sampled from a unit circle in the 2-D space, and the target is a uniform distribution on the unit square in the 2-D space (Fig. 2-(b)). We use a 3-layered CNN to approximate the generator in this case.

It is seen that the generative network struggles with transformation of a sequence of data points sampled from a distribution with a topological dimensionality of 1 (unit circle) into a distribution with a topological dimensionality of 2, and vice versa. It can be seen in Fig. 2, that when transforming a unit circle to a unit square, the generated samples lie inside the target distribution, but fail to cover the entire space.

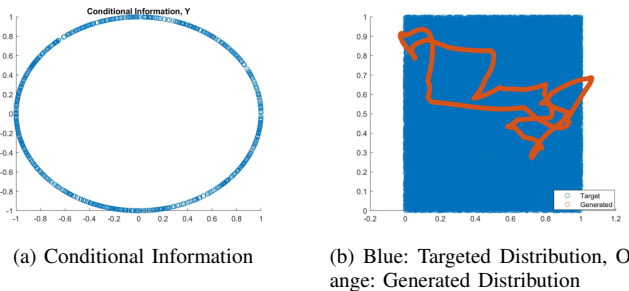
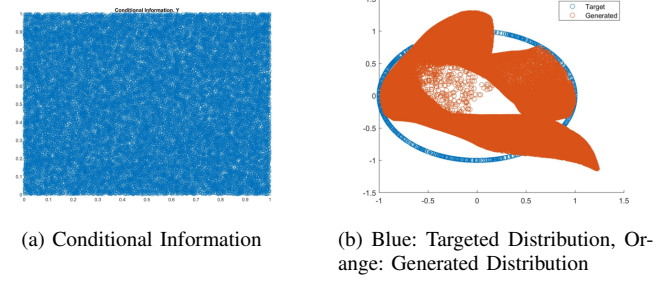


Fig. 2

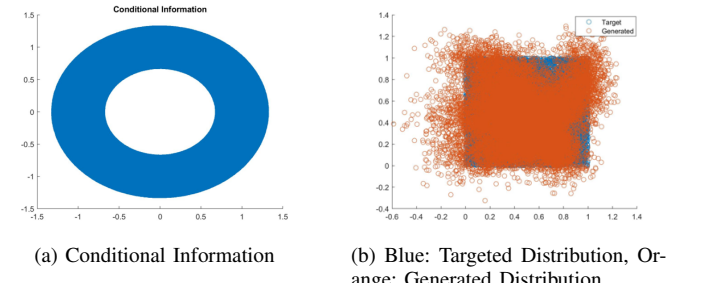
This is, however, solved by using a unit disk ( $x^2 + y^2 \in$



(a) Conditional Information  
(b) Blue: Targeted Distribution, Orange: Generated Distribution

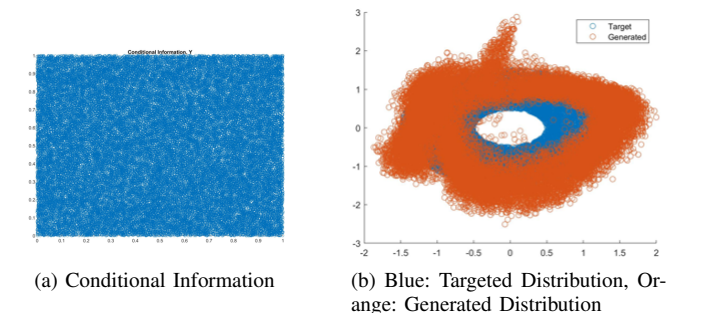
Fig. 3

$[1 - \epsilon, 1 + \epsilon]$ ), which has the same dimensionality as the unit square, as seen in Fig. 4. This goes to show that Generative networks are limited in generating a higher dimensional structure, when given an input with a lower dimension. For a reliable generation, dimensionality of the input sequence must be greater than or equal to that of the targeted distribution.



(a) Conditional Information  
(b) Blue: Targeted Distribution, Orange: Generated Distribution

Fig. 4



(a) Conditional Information  
(b) Blue: Targeted Distribution, Orange: Generated Distribution

Fig. 5

Later we see that this phenomenon is also observed in our implementations, as we require the use of a generated hidden space whose dimension is lower than that of the conditional information, in order to achieve optimal performance.

### III. PROBLEM FORMULATION

Consider  $L$  sensors surveilling an area of interest. We wish to detect/recognize targets,  $O = \{o_1, o_2, \dots, o_I\}$  given the data collected by the sensors. Let the  $n^{th}$  observation from the  $l^{th}$  sensor be denoted by,  $x_n^l = \{x_{nq}^l\}_{q=1 \dots d_l}$ . Let  $\mathbf{X}_{d_l \times N}^l =$

$\{\mathbf{x}_n^l\}_{n=1\dots N}$  be the set of  $N$  observations made by the  $l^{th}$  sensor.

We first seek to discover a hidden common space<sup>1</sup>  $\mathbf{H}_{d_H \times N}$ , of features captured by and hence present in the  $L$  sensors. Since it is unknown a priori, its structure may include shared and non-shared features captured by the sensors. We refer to the non-shared features of specific sensors, as private. Given a hidden space, this thus amounts to being able to select from each sensor the optimal set of features for classification via a selection matrix,  $\mathbf{S}^l$ ,

$$\forall l \in \{1, \dots, L\}, \quad \mathbf{F}_{d \times N}^l = \mathbf{S}_{d \times d_H}^l \mathbf{H}_{d_H \times N}. \quad (4)$$

Since the hidden space represents the information shared by the sensors, there must also exist a mapping,  $\mathbf{G}^l : \mathbf{X}^l \rightarrow \mathbf{H}$  such that,

$$\forall l \in \{1, \dots, L\}, \quad \hat{\mathbf{H}}_{d_H \times N}^l = \mathbf{G}^l(\mathbf{X}_{d_l \times N}^l) \approx \mathbf{H}_{d_H \times N} \quad (5)$$

From Equations 4 and 5 we have,

$$\forall l \in \{1, \dots, L\}, \quad \mathbf{F}_{d \times N}^l = \mathbf{S}_{d \times d_H}^l [(\mathbf{G}^l(\mathbf{X}^l))_{d_H \times N}]. \quad (6)$$

The existence of such a hidden space makes it possible to detect damaged sensors, and safeguard the system performance against them. When the  $l^{th}$  sensor is damaged, representative features for that sensor are reconstructed from the hidden space via the selection operator,  $\mathbf{F}^l = \mathbf{S}^l \mathbf{H}$ . Following the feature extraction, a linear classifier,  $c_i^l(\mathbf{F}^l) = w_i^{lT} \mathbf{F}^l + b_i^l$ , is used to determine the classification score for the  $i^{th}$  object as seen by the  $l^{th}$  sensor. The probability of occurrence of this object is then determined as,

$$P^l(o_i^l) = \frac{\exp(w_i^{lT} \mathbf{F}^l + b_i^l)}{\sum_{m=1}^L \exp(w_m^{lT} \mathbf{F}^l + b_m^l)}. \quad (7)$$

Finally, given these probability reports,  $R^l = \{P^l(o_i^l)\}$ , the objective is to determine the fused probability report  $R^f = \{P^f(o_i)\}$ , which is achieved using a special case of Event Driven Fusion [9], [10].

#### IV. PROPOSED APPROACH

As discussed in the previous section, the hidden space,  $\mathbf{H}$ , can be estimated from the  $l^{th}$  sensor observations as,  $\hat{\mathbf{H}}^l = \mathbf{G}^l(\mathbf{X}^l)$ . The mapping  $\mathbf{G}^l$  is approximated by a neural network and is realized as the generator of a Conditional Generative Adversarial Network (CGAN), that generates the estimate of the hidden space,  $\hat{\mathbf{H}}^l$ , while conditioned on the observations of the  $l^{th}$  sensor. Hence, we will have  $L$  generators that generate  $L$  estimates of the hidden space.

The desired output of these generators is to generate the estimate,  $\hat{\mathbf{H}}^l$ , such that,  $\forall l \in \{1, \dots, L\}$ ,  $\hat{\mathbf{H}}^l = \mathbf{G}^l(\mathbf{X}^l) \approx \mathbf{H}$ . On the other hand, the discriminator attempts to correctly identify the modality that the estimate of the hidden space was generated by. That is, it assigns a score  $D^l(\hat{h})$  as a probability that the estimate  $\hat{h}$ , was generated by  $\mathbf{G}^l$ . When

<sup>1</sup>In [3], such a space was referred to as an ‘information subspace’

updating the parameters for the  $l^{th}$  generator, the hidden space estimates generated by all the other generators are assumed to be the target space, and the  $l^{th}$  generator attempts to replicate these spaces, while at the same time attempting to generate an estimate that confuses the discriminator.

The standard formulation for the Generative Adversarial Network [19], [20] is known to have some instability issues [32]. Specifically, if the supports of the estimated hidden spaces are disjoint, which is highly likely when the inputs to the generators are coming from different modalities, a perfect discriminator is easily learned, and gradients for updating the generator may vanish. This issue was addressed in [32], and solved by using a Wasserstein GAN. So, using the sensor observations as the conditional information in the WGAN formulation [32], we have,

$$\begin{aligned} & \min_{\mathbf{G}^l} \max_{\mathbf{D}} \sum_{l=1}^L V(\mathbf{G}^l, \mathbf{D}), \\ V(\mathbf{G}^l, \mathbf{D}) &= \sum_{\substack{m=1 \\ m \neq l}}^L \{\mathbb{E}_{\mathbf{G}^m(x^m) \sim \mathbb{P}_H} [D^m(\mathbf{G}^m(x^m))] \\ &\quad - \mathbb{E}_{x^l \sim \mathbb{P}_{\mathbf{X}^l}} [D^l(\mathbf{G}^l(x^l))]\}. \end{aligned} \quad (8)$$

The discriminator  $\mathbf{D}$ , in the above formulation is required to be compact and  $K$ -Lipschitz. This is done by clamping the weights of the discriminator to a fixed box (eg.  $\theta_d \in [-0.01, 0.01]$ ) [32]. The discriminator is updated once after every generator update. That is, for  $L$  sensors, the discriminator is updated  $L$  times for one update to the  $l^{th}$  generator (see Algorithm 1). While this causes the estimates to be close to each other, it does not guarantee that the generated hidden spaces share the same basis.

A similar idea toward finding a common representation between multiple modalities was very recently and independently proposed in [31]. In this paper the authors attempt to find a common latent space between text and image modalities in order to perform image/text retrieval. Given a query from the image modality, the image is transformed into the latent common space, and the text with closest representation is retrieved.

In our work, we additionally ensure that the hidden space estimates share a common basis, enforcing as best can be done, a common subspace. These hidden estimates are later exploited in detecting damaged sensors on the basis of their similar operation, thus making the common subspace constraint important. To that end, we exploit an important property of commutation between the operators that are responsible for transforming the data into the common subspace.

**Definition 1.** *Linear operators  $\mathbf{A} \in \mathbb{R}^{nxn}$  and  $\mathbf{B} \in \mathbb{R}^{nxn}$  are said to commute if,*

$$[\mathbf{A}, \mathbf{B}] = \mathbf{AB} - \mathbf{BA} = 0. \quad (9)$$

**Theorem 1.** [24], [25] *If  $\mathbf{A} \in \mathbb{R}^{nxn}$  and  $\mathbf{B} \in \mathbb{R}^{nxn}$  are commuting linear operators, they share common eigenvectors.*

*Proof.* Consider an eigenbasis of  $\mathbf{A}$ ,  $\mathcal{V} = \{v_i\}$ , with  $\lambda_i$  the

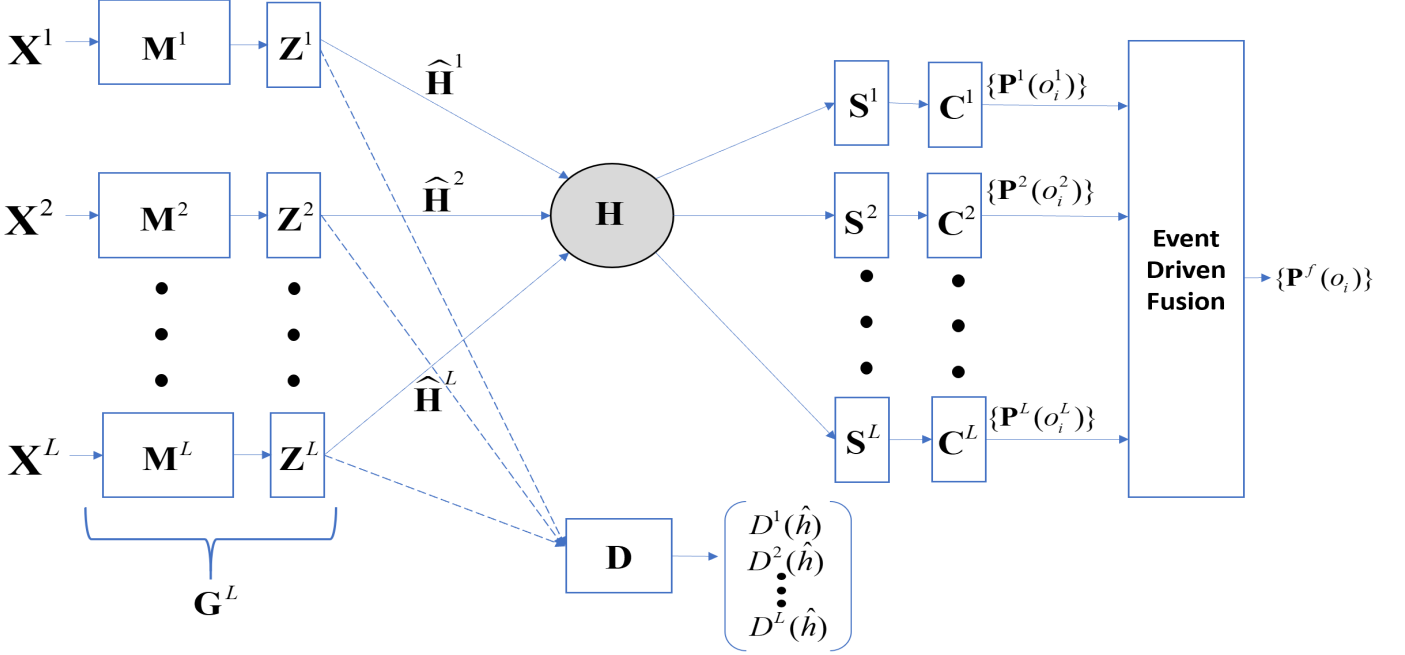


Fig. 6: Block diagram of the proposed approach for sensor fusion

eigenvalue associated to  $v_i$ . Then for any  $v_i$ ,

$$\mathbf{A}\mathbf{B}v_i = \mathbf{B}\mathbf{A}v_i = \lambda_i \mathbf{B}v_i, \quad (10)$$

i.e., if  $\mathbf{B}v_i \neq 0$ ,  $\mathbf{B}v_i$  is an eigenvector of  $\mathbf{A}$ , associated to the same eigenvalue as  $v_i$ ,  $\lambda_i$ .  $\square$

**Theorem 2.** [24], [25] If  $\mathbf{A} \in \mathbb{R}^{n \times n}$  and  $\mathbf{B} \in \mathbb{R}^{n \times n}$  are commuting operators that are also individually diagonalizable, they share a common eigenbasis.

*Proof.* If  $\mathbf{A}$  and  $\mathbf{B}$  are individually diagonalizable, they have  $n$ -distinct eigenvalues, i.e.  $\mathbf{A}$  can be diagonalized as,  $\mathbf{A} = \mathbf{P}\mathbf{D}_A\mathbf{P}^{-1}$ , where,  $\mathbf{D}_A$  is an  $n \times n$  diagonal matrix with eigenvalues of  $\mathbf{A}$  on the diagonal and  $\mathbf{P}$  is an  $n \times n$  matrix which has eigenvectors of  $\mathbf{A}$  as its columns. Since, both  $\mathbf{A}$  and  $\mathbf{B}$  share common eigenvectors (as seen in Theorem 1),  $\mathbf{B}$  can also be diagonalized as  $\mathbf{B} = \mathbf{P}\mathbf{D}_B\mathbf{P}^{-1}$ . Hence,  $\mathbf{A}$  and  $\mathbf{B}$  share a common eigenbasis.  $\square$

Let  $\mathbf{G}^l$  be composed of a Convolutional Neural Network,  $\mathbf{M}^l$ , followed by a fully connected layer,  $\mathbf{Z}^l$ . Note that the fully connected layer does not have any non-linear activation, and acts as a linear transform on  $\mathbf{M}^l(\mathbf{X}^l)$ . This thus results in,

$$\hat{\mathbf{H}}^l = \mathbf{Z}_{d_H \times d_H}^l [\mathbf{M}^l(\mathbf{X}^l)]_{d_H \times N}. \quad (11)$$

If the operators  $\mathbf{Z}^1, \dots, \mathbf{Z}^L$  commute, they will share a common eigenbasis. Furthermore, since the transformation,  $\mathbf{Z}^l[\mathbf{M}^l(\mathbf{X}^l)]$  lies in the range space of the operator,  $\mathbf{Z}^l$ ,  $\forall l$ ,  $\hat{\mathbf{H}}^l = \mathbf{Z}^l[\mathbf{M}^l(\mathbf{X}^l)]$  lie in a common subspace, due to the shared basis. While exact commutation cannot be guaranteed, we include a penalty term in the optimization to encourage the operators to commute, hence leading to operators that are ‘almost commuting’. Note that  $\mathbf{Z}^l$  must be a square matrix for validly enforcing the commutation cost as per Equation 9.

By including this with the GAN loss, Equation 8 becomes,

$$\min_{\mathbf{G}^l, \mathbf{Z}^l} \max_{\mathbf{D}} \sum_{l=1}^L \{V(\mathbf{G}^l, \mathbf{D}) + \gamma_2 \sum_{\substack{m=1 \\ m \neq l}}^L \|\mathbf{Z}^l, \mathbf{Z}^m\|^2\}. \quad (12)$$

While the CGAN network is expected to eventually generate samples that lie in the same subspace as the target data, even in the absence of this auxiliary loss, we observe that its inclusion nevertheless improves the generator performance tremendously, in spite of the fact that the target space is ill defined. Experiments show that including the commutation term speeds up convergence, and also yields better hidden space estimates.

#### A. Structure of the Hidden Space/Selection Operators

In addition to ensuring that the hidden space estimates generated by different modalities lie in a common subspace, it is also important to structure the hidden space in a way that it not only contains information shared between the sensor modalities, but also contains private information of individual modalities. This is especially important for heterogeneous sensors as they may provide additional information along with some common information. This conforms with the notion that no two sensors are completely similar or dissimilar. This is equivalent to structuring  $\mathbf{S}^l$  such that it selects features that are relevant to the  $l^{th}$  modality, while ignoring others. Such a structure can be achieved by encouraging the columns of the selection matrix to be close to zero. If the  $m^{th}$  column of  $\mathbf{S}^l$  is zeroed out, then the  $m^{th}$  feature in the hidden space,  $\mathbf{H}$ , does not contribute toward the  $l^{th}$  modality. This allows us to find the latent space,  $\mathbf{H}$ , that naturally separates information shared between different modalities from which is private to each modality. We implement this by minimizing the  $L_{\infty,1}$

norm, i.e.,  $\min_{\mathbf{S}^l} \|\mathbf{S}^l\|_{\infty,1}$ , where,

$$\|\mathbf{S}^l\|_{\infty,1} = \sum_j \max_i (|s_{ij}^l|). \quad (13)$$

This minimizes the sum of the maximum of each column in  $\mathbf{S}^l$ . Upon adding this term to the generator cost functional, we get,

$$\begin{aligned} \min_{\mathbf{G}^l, \mathbf{S}^l, \mathbf{Z}^l} \max_{\mathbf{D}} \sum_{l=1}^L \{ & V(\mathbf{G}^l, \mathbf{D}) + \gamma_1 \|\mathbf{S}^l\|_{\infty,1} \\ & + \gamma_2 \sum_{\substack{m=1 \\ m \neq l}}^L \|\mathbf{Z}^l, \mathbf{Z}^m\|^2 \} \end{aligned} \quad (14)$$

Notice that the above formulation has a trivial solution of setting  $\mathbf{S}^l = \mathbf{0}$ , and,  $\mathbf{Z}^l = \mathbf{0}$  for all  $l$ . In order to avoid this solution, we also optimize the classification based on the selected features,  $\mathbf{F}^l$ , for each modality, via the minimization of the cross-entropy loss. This ensures that the learned features,  $\mathbf{F}^l$ , are optimal for object detection/recognition, which is only possible if  $\mathbf{S}^l \neq \mathbf{0}$ , and,  $\mathbf{Z}^l \neq \mathbf{0}$ . Given the sensor observations,  $\mathbf{X}^l$ , and the classifier  $\mathbf{C}^l = \{c_i^l\}$ , the cross-entropy loss is computed as,

$$C_{LOSS}^l(\mathbf{F}^l) = \sum_{n=1}^N \sum_{i=1}^I -y_{ni} \log \sigma(c_i^l(\mathbf{f}_n^l)), \quad (15)$$

where,  $Y_n = \{y_{ni}\}$  is the ground truth for the  $n^{th}$  sample,  $\sigma$  is the soft-max function, and,  $\mathbf{f}_n^l = \mathbf{S}^l[\mathbf{G}^l(\mathbf{x}_n^l)]$ .

Finally, the optimization task is,

$$\begin{aligned} \min_{\mathbf{G}^l, \mathbf{Z}^l, \mathbf{S}^l, \mathbf{C}^l} \max_{\mathbf{D}} \mathcal{L}(\mathbf{G}^l, \mathbf{D}, \mathbf{Z}^l, \mathbf{S}^l, \mathbf{C}^l) \\ \mathcal{L}(\mathbf{G}^l, \mathbf{D}, \mathbf{Z}^l, \mathbf{S}^l, \mathbf{C}^l) = \sum_{l=1}^L \{ & V(\mathbf{G}^l, \mathbf{D}) + \gamma_1 \|\mathbf{S}^l\|_{\infty,1} \\ & + \gamma_2 \sum_{\substack{m=1 \\ m \neq l}}^L \|\mathbf{Z}^l, \mathbf{Z}^m\|^2 + \gamma_3 C_{LOSS}^l(\mathbf{F}^l), \end{aligned} \quad (16)$$

where,  $\gamma_1$ ,  $\gamma_2$ , and  $\gamma_3$  are hyper-parameters that control the contribution of different terms toward the optimization.

The necessary updates to train these networks are summarized in Algorithm 1. This setup learns the optimal features for classification  $\mathbf{F}^l$ , while driven by the existence of the hidden space  $\mathbf{H}$ , such that  $\mathbf{F}^l = \mathbf{S}^l \mathbf{H}$ . Due to the inclusion of the selection matrix  $\mathbf{S}^l$ , followed by the Classification Layer, note that hand-crafting of features as in [9], [10], is no longer required. The features of interest are learned and automatically selected by the optimization during the training phase. The effects of the different terms in Equation 16 on the determined hidden spaces are shown in Section V-B in Figures 11, 12, and 13.

### B. A Special Case of Event Driven Fusion

In order to fuse the individual decisions from the sensors we use a special case of Event Driven Fusion. Instead of defining feature events for each object as in [9], an event in this case is

the occurrence of the  $i^{th}$  object as seen by the  $l^{th}$  sensor,  $o_i^l$ . The  $l^{th}$  classifier,  $\mathbf{C}^l = \{c_i^l\}$ , provides the corresponding probability given the test sample,  $\mathbf{x}_t^l$ ,  $P_t^l(o_i^l) = \frac{\exp(c_i^l(\mathbf{f}_t^l))}{\sum_{m=1}^L \exp(c_m^l(\mathbf{f}_t^l))}$ , as previously discussed in Section III. Each sensor report is now represented as,  $R_t^l = \{P_t^l(o_i^l)\}$ , and the fused probability of occurrence of the  $i^{th}$  object as per the rules of Event Driven Fusion [9] is determined as,

$$\begin{aligned} P_t^f(o_i) = P_t(o_i^1, o_i^2, \dots, o_i^L) = & \rho \cdot P_{\text{MAX MI}}(o_i^1, o_i^2, \dots, o_i^L) \\ & + (1 - \rho) \cdot P_{\text{MIN MI}}(o_i^1, o_i^2, \dots, o_i^L), \end{aligned} \quad (22)$$

where  $\rho$  is a pseudo-measure of correlation between the sensor modalities. For making an informed decision in favor of an object, this formulation assumes all the modalities to be equally reliable. This is not always true in practice, as certain sensors may provide more discriminative information than others, and are hence more reliable. It is thus important to weigh the various sensor decisions by a Degree of Confidence (DoC). The DoC in the decisions made by the  $l^{th}$  sensor given the test sample,  $\mathbf{x}_t^l$ , is denoted by,  $DoC_t^l \in [0, 1]$ , where  $DoC_t^l = 0$  implies that the sensor observations do not provide any useful information about the target identity, and  $DoC_t^l = 1$  implies that information provided by the sensor is highly discriminative with respect to target classification. The individual sensor reports,  $R_t^l = \{P_t^l(o_i^l)\}$ , are now redefined as,

$$R_t^l = \{P_t^l(o_1^l), P_t^l(o_2^l), \dots, P_t^l(o_i^l), P_t^l(\text{unc}^l)\}, \quad (23)$$

where  $P_t^l(o_i^l) = DoC_t^l * P_t^l(o_i^l)$ , and  $P_t^l(\text{unc}^l) = 1 - DoC_t^l$  is the probability that the  $l^{th}$  sensor is uncertain about the target identity. The joint probability distribution for the new sensor reports is now rewritten as,

$$\begin{aligned} P_t(a^1, a^2, \dots, a^L) = & \rho \cdot P_{\text{MAX MI}}(a^1, a^2, \dots, a^L) \\ & + (1 - \rho) \cdot P_{\text{MIN MI}}(a^1, a^2, \dots, a^L), \end{aligned} \quad (24)$$

where,  $a^l \in \{o_1^l, o_2^l, \dots, o_i^l, \text{unc}^l\}$ , and the probability of occurrence of the  $i^{th}$  target is computed as,

$$\begin{aligned} P_t^f(o_i) = P_t((\bigwedge_{l=1}^L o_i^l) \bigvee_{m_1=1}^L (\text{unc}^{m_1} \bigwedge_{\substack{l=1 \\ l \neq m_1}}^L o_i^l) \\ \bigvee_{m_1, m_2=1}^L (\text{unc}^{m_1} \wedge \text{unc}^{m_2} \bigwedge_{\substack{l=1 \\ l \neq m_1 \\ l \neq m_2}}^L o_i^l) \\ \dots \bigvee_{m_{L-1}, m_L=1}^L (\bigwedge_{j=1}^{L-1} \text{unc}^{m_j} \bigwedge_{\substack{l=1 \\ \forall j, l \neq m_j}}^L o_i^l)), \end{aligned} \quad (25)$$

with a degree of confidence,  $DoC_t^f = 1 - P_t(\bigwedge_{l=1}^L \text{unc}^l)$ , in the fused decision.

For a 2D scenario (i.e. two sensors), the probability of occurrence of the  $i^{th}$  target is,

$$P_t^f(o_i) = P_t((o_i^1 \wedge o_i^2) \vee (\text{unc}^1 \wedge o_i^2) \vee (o_i^1 \wedge \text{unc}^2)), \quad (26)$$

with a degree of confidence,  $DoC_t^f = 1 - P(\text{unc}^1 \wedge \text{unc}^2)$ , in the fused decision. This formulation takes into account the

---

**Algorithm 1:** Training the CGAN system

Let  $\{\theta_{g_l}^q\}_{q \in \{1, \dots, Q\}}$  be the parameters for the  $q^{th}$  layer of the  $l^{th}$  generator, and  $\mathbf{y}_q$  be the output of that layer.

$\mathbf{y}^Q = \mathbf{Z}^l[\mathbf{M}^l(\mathbf{X}^l)]$ , and,  $\mathbf{y}^{Q-1} = \mathbf{M}^l(\mathbf{X}^l)$ .

Similarly, Let  $\{\theta_d^r\}_{r \in \{1, \dots, R\}}$  be the parameters of the  $r^{th}$  layer of the discriminator and  $\mathbf{z}^r$  be the output of that layer.

- for  $j$  in 1 : Number of Iterations

- for  $l$  in 1 :  $L$

- \* Update the discriminator network,

$$\theta_d^{r(j)} \leftarrow \theta_d^{r(j-1)} + \mu_D \left\{ \frac{d\mathcal{L}(\mathbf{G}^l, \mathbf{D}, \mathbf{Z}^l, \mathbf{S}^l, \mathbf{C}^l)}{d\mathbf{z}^R} \frac{d\mathbf{z}^R}{d\mathbf{z}^{R-1}} \dots \frac{d\mathbf{z}^{r+1}}{d\theta_d^r} \right\} \quad (17)$$

- \* Update the  $l^{th}$  generator network,

$$\mathbf{C}^{l(j)} \leftarrow \mathbf{C}^{l(j-1)} - \mu_G \left\{ \frac{d\mathcal{L}(\mathbf{G}^l, \mathbf{D}, \mathbf{Z}^l, \mathbf{S}^l, \mathbf{C}^l)}{d\mathbf{C}^l} \right\} \quad (18)$$

$$\mathbf{S}^{l(j)} \leftarrow \mathbf{S}^{l(j-1)} - \mu_G \left\{ \frac{d\mathcal{L}(\mathbf{G}^l, \mathbf{D}, \mathbf{Z}^l, \mathbf{S}^l, \mathbf{C}^l)}{d\mathbf{C}^l(\mathbf{F}^l)} \frac{d\mathbf{C}^l(\mathbf{F}^l)}{d\mathbf{F}^l} \frac{d\mathbf{F}^l}{\mathbf{S}^l} + \frac{d\mathcal{L}(\mathbf{G}^l, \mathbf{D}, \mathbf{Z}^l, \mathbf{S}^l, \mathbf{C}^l)}{d\mathbf{S}^l} \right\} \quad (19)$$

$$\begin{aligned} \mathbf{Z}^{l(j)} &\leftarrow \mathbf{Z}^{l(j-1)} - \mu_G \left\{ \frac{d\mathcal{L}(\mathbf{G}^l, \mathbf{D}, \mathbf{Z}^l, \mathbf{S}^l, \mathbf{C}^l)}{d\mathbf{C}^l(\mathbf{F}^l)} \frac{d\mathbf{S}^l(\mathbf{Z}^l[\mathbf{M}^l(\mathbf{X}^l)])}{d\mathbf{Z}^l[\mathbf{M}^l(\mathbf{X}^l)]} \frac{d\mathbf{C}^l(\mathbf{F}^l)}{d\mathbf{F}^l} \frac{d\mathbf{Z}^l[\mathbf{M}^l(\mathbf{X}^l)]}{d\mathbf{Z}^l} + \frac{d\mathcal{L}(\mathbf{G}^l, \mathbf{D}, \mathbf{Z}^l, \mathbf{S}^l, \mathbf{C}^l)}{d\mathbf{Z}^l} \right\} \\ \theta_{g_l}^{q(j)} &\leftarrow \theta_{g_l}^{q(j-1)} - \mu_G \left\{ \frac{d\mathcal{L}(\mathbf{G}^l, \mathbf{D}, \mathbf{Z}^l, \mathbf{S}^l, \mathbf{C}^l)}{d\mathbf{C}^l(\mathbf{F}^l)} \frac{d\mathbf{C}^l(\mathbf{F}^l)}{d\mathbf{F}^l} \frac{d\mathbf{S}^l(\mathbf{G}^l(\mathbf{X}^l))}{d\mathbf{G}^l(\mathbf{X}^l)} \frac{d\mathbf{G}^l(\mathbf{X}^l)}{d\mathbf{y}^{Q-1}} + \frac{d\mathcal{L}(\mathbf{G}^l, \mathbf{D}, \mathbf{Z}^l, \mathbf{S}^l, \mathbf{C}^l)}{d\mathbf{G}^l(\mathbf{X}^l)} \frac{d\mathbf{G}^l(\mathbf{X}^l)}{d\mathbf{y}^{Q-1}} \right\} \left\{ \frac{d\mathbf{y}^{Q-1}}{d\mathbf{y}^{Q-2}} \dots \frac{d\mathbf{y}^{q+1}}{d\theta_{g_l}^q} \right\} \end{aligned} \quad (20)$$

$$\theta_{g_l}^{q(j)} \leftarrow \theta_{g_l}^{q(j-1)} - \mu_G \left\{ \frac{d\mathcal{L}(\mathbf{G}^l, \mathbf{D}, \mathbf{Z}^l, \mathbf{S}^l, \mathbf{C}^l)}{d\mathbf{C}^l(\mathbf{F}^l)} \frac{d\mathbf{C}^l(\mathbf{F}^l)}{d\mathbf{F}^l} \frac{d\mathbf{S}^l(\mathbf{G}^l(\mathbf{X}^l))}{d\mathbf{G}^l(\mathbf{X}^l)} \frac{d\mathbf{G}^l(\mathbf{X}^l)}{d\mathbf{y}^{Q-1}} + \frac{d\mathcal{L}(\mathbf{G}^l, \mathbf{D}, \mathbf{Z}^l, \mathbf{S}^l, \mathbf{C}^l)}{d\mathbf{G}^l(\mathbf{X}^l)} \frac{d\mathbf{G}^l(\mathbf{X}^l)}{d\mathbf{y}^{Q-1}} \right\} \left\{ \frac{d\mathbf{y}^{Q-1}}{d\mathbf{y}^{Q-2}} \dots \frac{d\mathbf{y}^{q+1}}{d\theta_{g_l}^q} \right\} \quad (21)$$


---

potential uncertainties in the decisions made by individual sensors. Figure 7 shows the joint distribution to be determined in a 2D case.

$D_t^1$	$D_t^2$	$DoC_t^2.P_t^2(o_1^2)$	$DoC_t^2.P_t^2(o_2^2)$	$P_t^2(unc^2)$
$DoC_t^1.P_t^1(o_1^1)$	$P(o_1^1, o_2^1)$	$P(o_1^1, o_2^2)$	$P(o_1^1, unc^2)$	
$DoC_t^1.P_t^1(o_2^1)$	$P(o_2^1, o_1^2)$	$P(o_2^1, o_2^2)$	$P(o_2^1, unc^2)$	
$P_t^1(unc^1)$	$P(unc^1, o_1^2)$	$P(unc^1, o_2^2)$	$P(unc^1, unc^2)$	

Fig. 7: Fused joint probability distributions when accounting for the uncertain event. The joint distribution is determined following the rules of Event Driven Fusion.

The degree of confidence in the  $l^{th}$  sensor for classification of the test sample,  $\mathbf{x}_t^l$ , is determined as,

$$DoC_t^l = (1 - p_D(\hat{\mathbf{h}}_t^l)).Acc_{train}^l, \quad (27)$$

where,  $p_D(\hat{\mathbf{h}}_t^l)$  is the probability of damage for the  $l^{th}$  sensor given the test sample,  $\mathbf{x}_t^l$  (discussed in detail in the next subsection), and  $Acc_{train}^l$  is the training accuracy of the  $l^{th}$  sensor. The training accuracy in Equation 27 represents prior information about the discrimination power of the sensor, while  $(1 - p_D(\hat{\mathbf{h}}_t^l))$  represents the sensor condition at the time of operation/testing.

### C. Sensor Failure Detection

Since  $\mathbf{H}$  is designed so that it be common for all the sensors, it may be used to detect a damaged sensor.

1) *Cross-Sensor Tracking*: The estimate  $\hat{\mathbf{H}}^m$ , based on erroneous observations, will significantly deviate from the estimates from normal observations (i.e. sensors that are not damaged),  $\hat{\mathbf{H}}^l, l \neq m$ . This allows detection of damage in a

sensor during the testing phase. The  $m^{th}$  sensor is said to be damaged if,

$\forall j, l \neq m$ ,

$$\sum_{\substack{l=1 \\ l \neq m}}^L \mathcal{I}(\|\hat{\mathbf{h}}_t^m - \hat{\mathbf{h}}_t^l\|^2 > T) \geq \begin{cases} \frac{L-1}{2}, & \text{if } L \text{ is odd,} \\ \frac{L}{2} - 1, & \text{if } L \text{ is even.} \end{cases}$$

$$\text{And, } \sum_{\substack{j,l=1 \\ j,l \neq m}}^L \mathcal{I}(\|\hat{\mathbf{h}}_t^j - \hat{\mathbf{h}}_t^l\|^2 < T) \geq \begin{cases} \frac{L-1}{2}, & \text{if } L \text{ is odd,} \\ \frac{L}{2} - 1, & \text{if } L \text{ is even.} \end{cases} \quad (28)$$

where,  $\mathcal{I}(.)$  is the indicator function,  $T$  is a threshold value determined from the training data, and  $\hat{\mathbf{h}}_t^l$  is the estimated hidden space given the observation  $\mathbf{x}_t^l$ . The limitation with this approach is that we can only detect up to  $\frac{L-1}{2} / \frac{L}{2} - 1$  damaged sensors.

2) *Hierarchical Clustering*: A faulty sensor can also be detected by comparing the hidden space generated by the test sample with that generated from training data. One way to proceed is by clustering functional sensor observations (from training data), and verify whether the hidden space estimate generated by the test sample can be associated to any of these clusters. The concatenation of the training data,  $\hat{\mathbf{H}}_{d \times LN}^C = \{\hat{\mathbf{H}}^1, \hat{\mathbf{H}}^2, \dots, \hat{\mathbf{H}}^L\}$ , is first used to construct a clustering tree based on an Agglomerative approach (see Algorithm 2). The probability of damage of the  $l^{th}$  sensor is then computed as,

$$p_D(\hat{\mathbf{h}}_t^l) = \frac{d_{lev}}{\max_v d_v}, \quad (29)$$

where,  $d_v$  is the cut-off distance at clustering level  $v$ , and,

$$lev = \arg \min v$$

$$s.t. \exists j \in \{1, \dots, J_{lev}\}, \hat{\mathbf{h}}_t^l \in Z_{lev}^j, \quad (30)$$

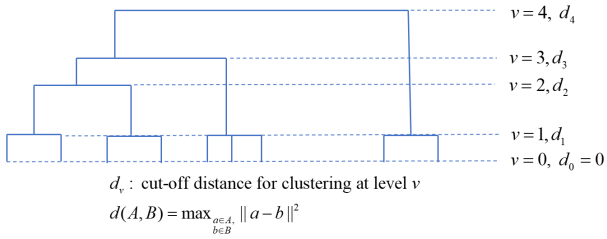


Fig. 8: A clustering tree created using Hierarchical Clustering (Agglomerative Clustering)

$v = 1, \dots, V$  are the clustering levels,  $J_v$  is the number of clusters at level  $v$ , and  $Z_v^j$  is the  $j^{th}$  cluster at level  $v$ . This is a measure of how quickly the hidden space estimate,  $\hat{h}_t^l$ , can be clustered with the training data.

The  $l^{th}$  sensor is said to be damaged if,

$$p_D(\hat{h}_t^l) > T, \quad (31)$$

where,  $T$ , is a threshold value which will depend on the dataset, types of sensors, SNR, etc. In our evaluation, we compute the optimal thresholds at different SNRs for the training data, and these thresholds are later used during the testing phase in order to determine the state of a sensor. This probability measure is also used in Equation 27, in order to adapt the DoC based on the sensor condition in a functional mode. If the sensor is damaged, the representative features are generated using the selection matrix as,

$$\hat{f}_t^l = S^l \left( \frac{\sum_{m \in \Gamma} DoC_t^m \cdot \hat{h}_t^m}{\sum_{m \in \Gamma} DoC_t^m} \right), \quad (32)$$

where,  $\Gamma$  is the set of working sensors.

**Algorithm 2:** Hierarchical Clustering (Agglomerative Clustering)

- Initialize clusters at  $v = 0$ :  $\mathcal{C}_0 = \{Z_0^j = \{h_j\}, j = 1 \dots L.N\}$
- while Number of Clusters  $> 1$ :
  - $v = v + 1$
  - Among all cluster pairs,  $\{Z_{v-1}^r, Z_{v-1}^s\}$ , find the one, say  $\{Z_{v-1}^i, Z_{v-1}^j\}$ , such that:

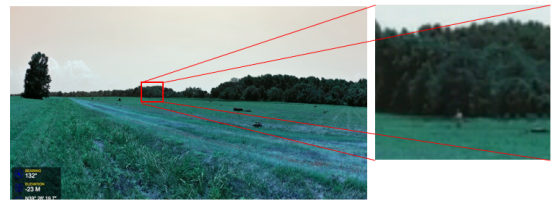
$$d(Z_{v-1}^i, Z_{v-1}^j) = \min_{r,s} d(Z_{v-1}^r, Z_{v-1}^s), \quad (33)$$

where,  $d(\cdot)$  is a measure of dissimilarity.

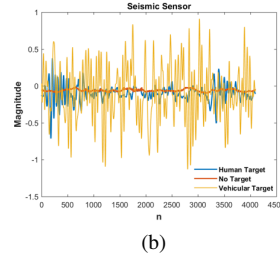
- Assign  $Z_v^q = Z_{v-1}^i \cup Z_{v-1}^j$
- Get new clustering:  $\mathcal{C}_v = \{(\mathcal{C}_{v-1} - \{Z_{v-1}^i, Z_{v-1}^j\}) \cup Z_v^q\}$

## V. EXPERIMENTS AND RESULTS

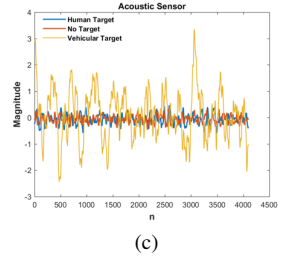
We validate our proposed approach by running experiments on two different datasets. The first dataset we use is pre-collected data from a network of seismic, acoustic, and imaging sensors deployed in a field, where people/vehicles were walking/driven around in specified patterns. Details about this sensor setup and experiments can be found in [26]. This dataset has been previously used for target detection in [9], [14], [27],



(a)



(b)



(c)

Fig. 9: (a): Sample video frame with a human target, (b): Sample seismic sensor observations for human target, vehicular target, and no target cases, (c): Sample acoustic sensor observations for human target, vehicular target, and no target cases.

[28]. Here, we use this dataset to classify between human targets, vehicular targets, and no targets. Some data samples from the sensors can be seen in Figure 9. This will be referred to as ‘Dataset-1’ in the following discussions.

For our second experiment, we select two sensors, namely a Radar sensor and a telescopic optical sensor, for one (latter) of which we have acquired real data. For technical reasons, our Radar measurements were never co-measured with the optical data, and so we use MATLAB Simulink in order to simulate the radar responses. Both sensors are ideally synchronized when observing a given target, which in our case, can be any object in outer space, such as satellite or space debris. Each generated radar signal over one second is correlated with two telescopic images. Samples for objects with different velocities, cross-sections, ranges, and aspect-ratios are then generated.

Object classes are defined in the same way as in [10], based on events on the feature values. Note that these events are no longer required for training purposes, and are only used for the purposes of labeling the data. For the radar, we use the features, velocity ( $v$ ), cross-section ( $cs$ ), and range ( $r$ ), and the events are defined as,

$$\begin{aligned} a_1^v : 0 \leq v \leq 10 \text{ m/s}, \quad a_2^v : 15 \text{ m/s} \leq v \leq 35 \text{ m/s}, \\ a_1^r : 0 < r \leq 300 \text{ m}, \quad a_2^r : 300 \text{ m} < r, \\ a_1^{cs} : 0 < cs \leq 20 \text{ m}^2, \quad a_2^{cs} : 15 \text{ m}^2 \leq cs \leq 50 \text{ m}^2. \end{aligned} \quad (34)$$

From the telescopic imaging sensor, the features, displacement ( $d$ ) and aspect ratio ( $AR$ ) define the following events,

$$\begin{aligned} a_1^d : 0 \leq d \leq 60 \text{ pixels}, \quad a_2^d : 90 \text{ pixels} \leq d \leq 210 \text{ pixels}, \\ a_1^{ar} : 0 < AR \leq 1.5, \quad a_2^{ar} : 1.5 < AR. \end{aligned} \quad (35)$$

Furthermore, the objects for classification are defined in terms

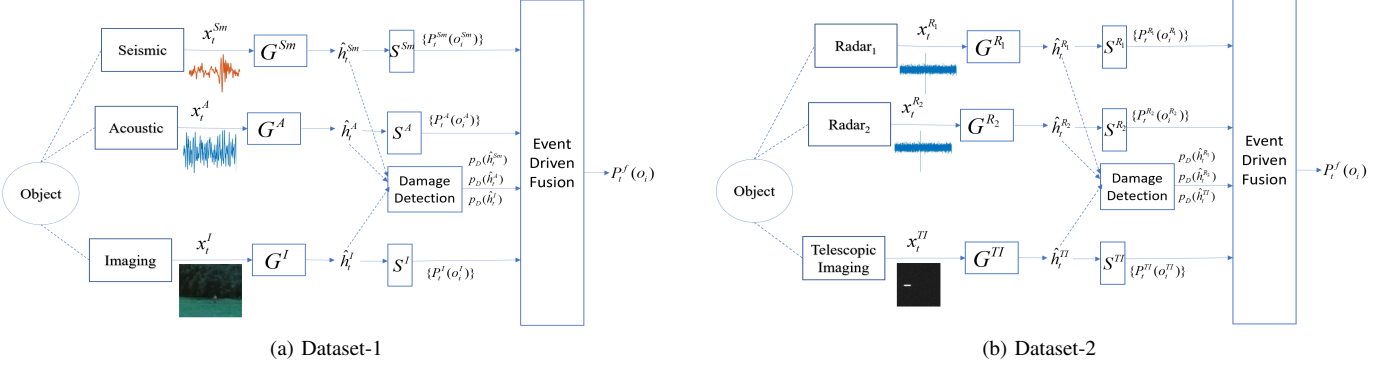


Fig. 10: Block Diagram of Implementation

of these events as,

$$o_1 : \{a_1^r \wedge [(a_2^v \wedge a_2^d) \vee (a_2^{cs} \vee a_2^{ar})]\} \quad (36)$$

$$o_2 : \{a_1^v \wedge a_1^d \wedge a_2^r \wedge a_1^{cs} \wedge a_1^{ar}\} \quad (37)$$

This will be referred to as ‘Dataset-2’ in the following discussions.

#### A. Implementation Details

Figure 10-(a) shows the detailed block diagram for implementation of the discussed approach on Dataset-1. As noted earlier we no longer require handcrafted features and event definitions as in [9], [10], since we let the generative structure (see Figure 10) guide the learning of features. Similarly, the block diagram for implementation of this system on Dataset-2 can be seen in Figure 10-(b). The output of the  $l^{th}$  generator,  $G^l$ , for a test sample,  $x_t^l$ , is a  $d_H$ -dimensional estimate of the hidden space,  $\hat{h}_t^l$ . This hidden space is also used to detect potential damages to the sensors deployed. The optimal features  $f_t^l$ , are subsequently selected by each sensor for making decisions on target identities via the selection matrix  $S^l$ . The decisions are then fed into the fusion system which synthesizes a decision on the basis of the rules discussed in Section IV-B.

The generator network uses 1-D convolutions in case of seismic/acoustic and radar modalities, and 2-D convolutions in case of the imaging sensors. We use a 6 layered Neural Network, with 2x2 max pooling layer after the 2<sup>nd</sup> and 4<sup>th</sup> layer. ReLU activation is applied after every convolutional layer. The first 4 layers are convolutional, while the last two are fully connected. The first two convolutional layers use a filter size of 5 and the next two use a filter size of 3. The first fully connected layer is used to transform the output of the convolutional layers into a  $d_H$  dimensional representation. All the layers preceding the final fully connected layer approximate the mapping  $M^l$ , while the final layer approximates the operator  $Z^l$ , and transforms the data into a common subspace.

In determining the dimension of the hidden space, we search over values ranging from  $d = 50$  to  $d = 5000$ . For Dataset-1 we find the best performance at  $d = 500$ , while for Dataset-2,  $d = 700$ . In both cases we observe that at best performance,  $d \ll d_l$ .

#### B. Performance Analysis

TABLE I: Performance Comparison for the First Dataset

Method	Accuracy (Dataset-1)	Accuracy (Dataset-2)
Seismic Sensor	93.62 %	-
Acoustic Sensor	68.71 %	-
Imaging Sensor	90.33 %	-
Radar Sensor 1	-	89.33 %
Radar Sensor 2	-	86.73 %
Telescopic Imaging Sensor	-	83.57 %
Feature Concatenation	88.13 %	86.45 %
Dissimilar Sensor Fusion	91.61 %	-
Similar + Dissimilar Sensor Fusion	-	89.63 %
Dempster-Shafer Fusion	88.77 %	87.30 %
Event Driven Fusion (Without using GAN structure) [9], [10]	92.04 %	90.36 %
Canonical Correlation Analysis [28]	86.64 %	85.69 %
Discriminant Analysis	91.33 %	88.21 %
Dictionary Learning [29]	94.46 %	93.77 %
Hidden Space Generated by GAN	95.13 %	91.13 %
<b>Event Driven Fusion + GAN</b>	<b>97.79 %</b>	<b>95.34 %</b>

Table I shows the performance of different techniques as compared with the proposed approach of using a Generative Adversarial Network to learn optimal features, which are then used for target detection. All sensors are assumed to be working normally in Table I. Comparisons are carried out with approaches that perform fusion at the decision level, as well as those that seek a hidden space for fusion. We find that using the individual sensor features (whose learning is driven by the existence of a structured hidden space) for classification and performing decision level fusion on these classifications yields better performance relative to those based solely on the hidden space. For the evaluation of Model Based Fusion approaches

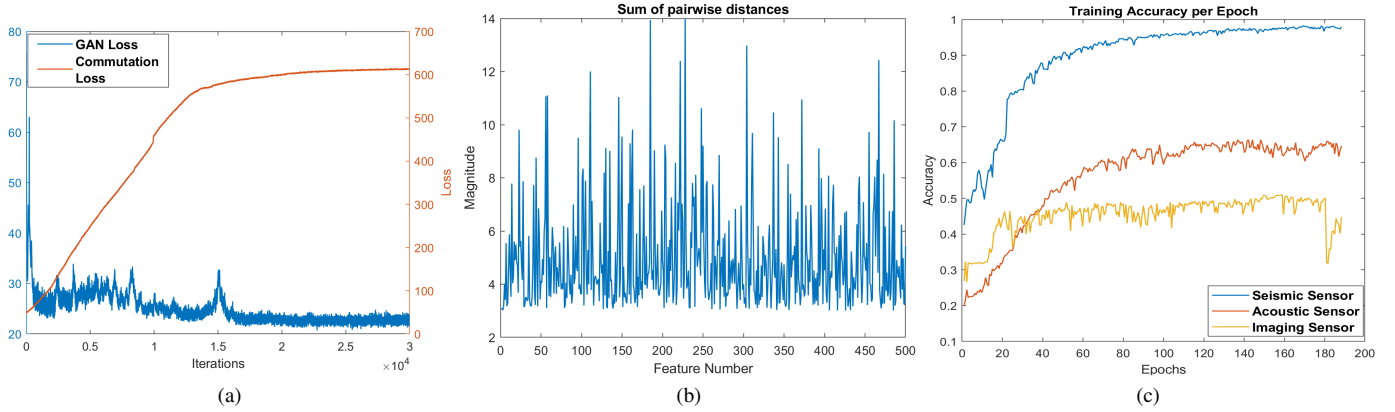


Fig. 11: (a): Optimization Losses, (b): Sum of pairwise distances between hidden estimates, (c): Training Accuracies/Epoch when GAN Loss is optimized in tandem with classification loss

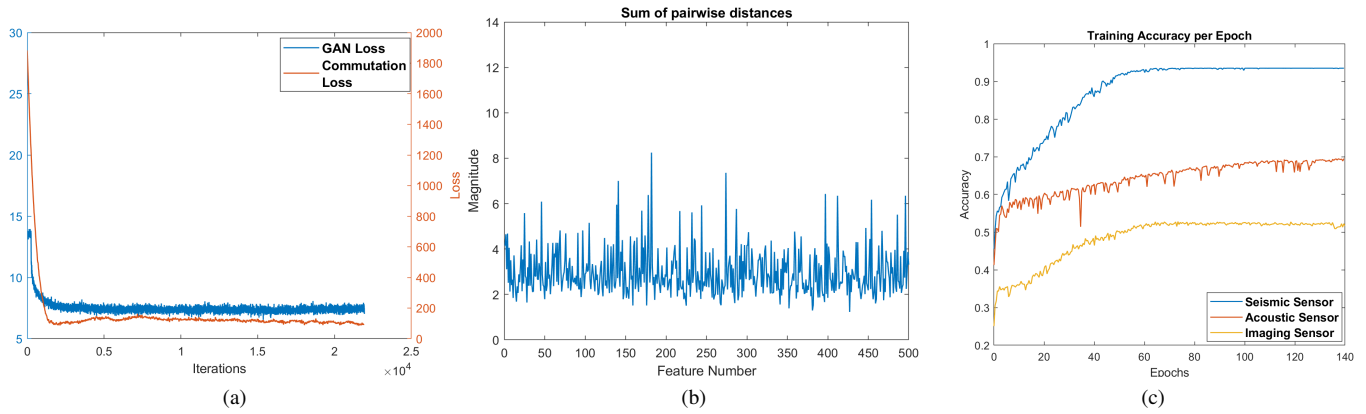


Fig. 12: (a): Optimization Losses, (b): Sum of pairwise distances between hidden estimates, (c): Training Accuracies/Epoch when commutation term is included with the GAN and classification term

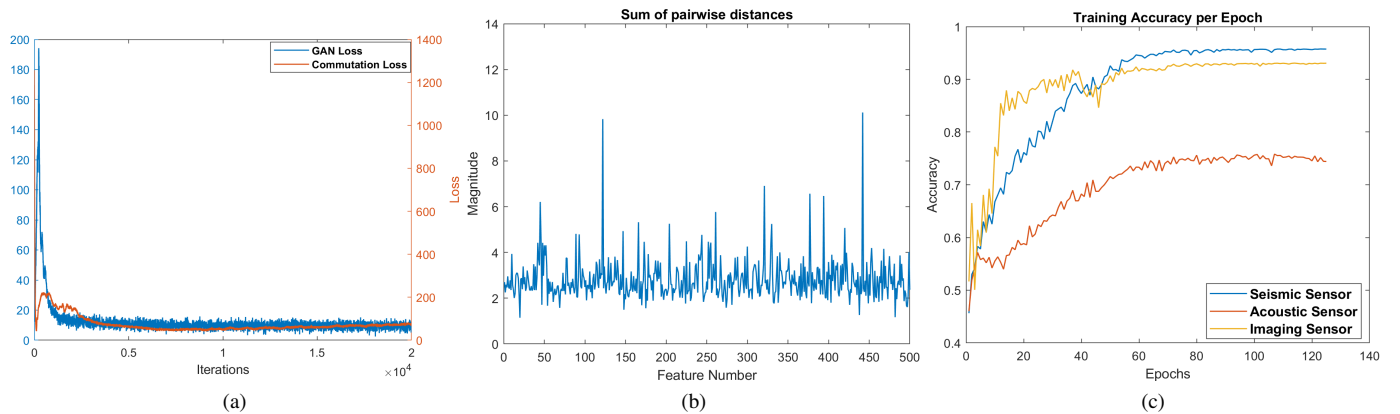
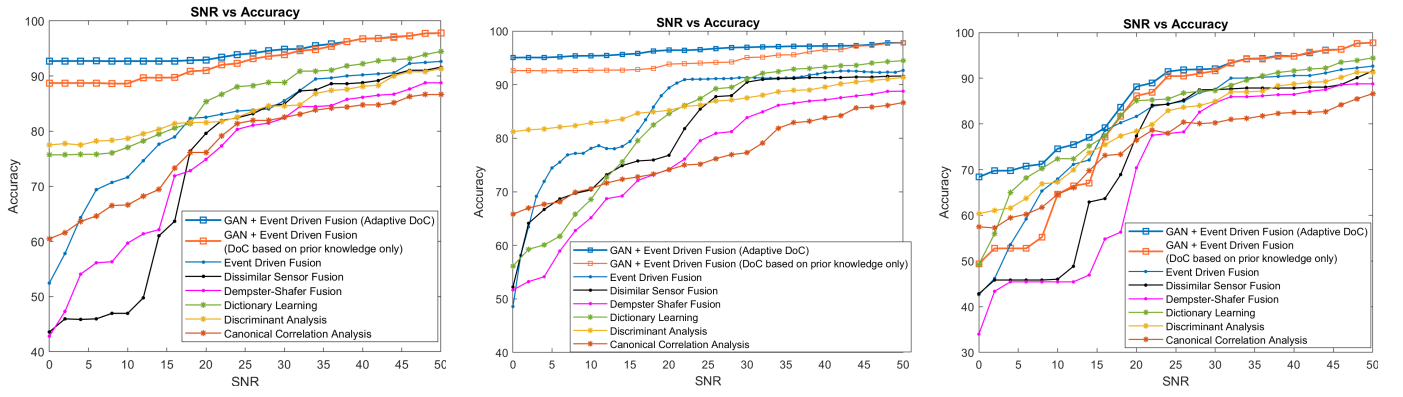


Fig. 13: (a): Optimization Losses, (b): Sum of pairwise distances between hidden estimates, (c): Training Accuracies/Epoch when all terms in Equation 16 are active.

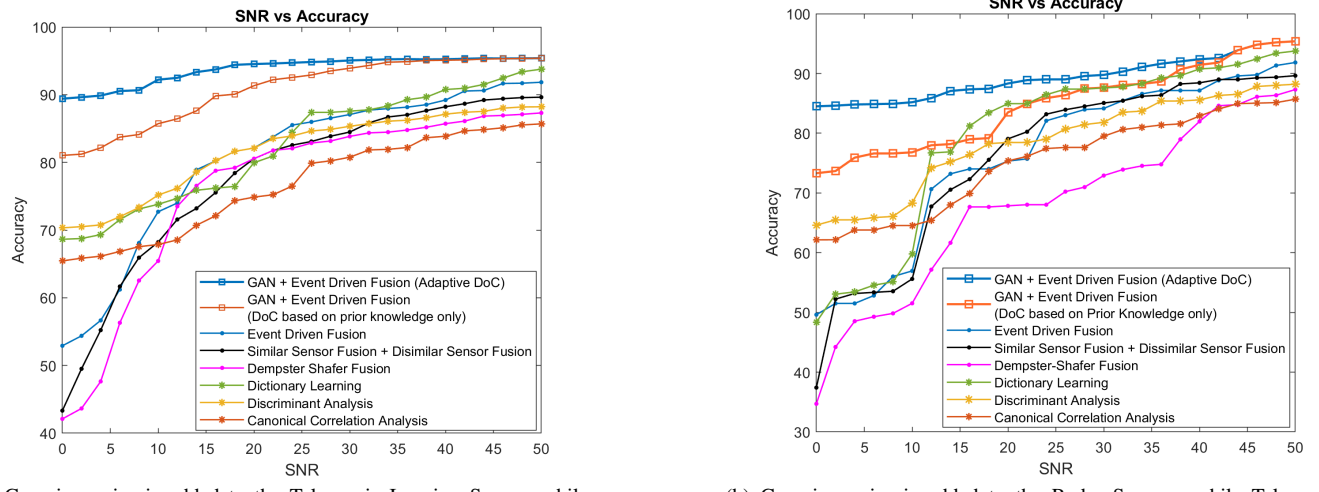


(a) Gaussian noise is added to Seismic and Acoustic Sensor, while Imaging data is assumed to be clean.

(b) Gaussian noise is added to Imaging and Acoustic Sensor, while Seismic data is assumed to be clean.

(c) Gaussian noise is added to Seismic and Imaging Sensor, while Acoustic data is assumed to be clean.

Fig. 14: Comparison of the proposed technique (GAN + Event Driven Fusion) with existing techniques for Dataset-1.



(a) Gaussian noise is added to the Telescopic Imaging Sensor, while Radar data is assumed to be clean.

(b) Gaussian noise is added to the Radar Sensors, while Telescopic Imaging data is assumed to be clean.

Fig. 15: Comparison of the proposed technique (GAN + Event Driven Fusion) with existing techniques for Dataset-2.

(see Section II-A), the dissimilar sensor setting is considered for Dataset-1 as all three sensors are different. On the other hand, for Dataset-2, the two radars are first combined using similar sensor fusion and the result of this is combined with the telescopic sensor using dissimilar sensor fusion.

We also compare the effects of different losses in our objective. First we implement a system which uses an Adversarial setup, along with the classification losses, i.e.,  $\gamma_1$ , and  $\gamma_2$  in Equation 16 are set to 0. The losses are seen in Figure 11-(a). The blue plot represents the negative of the discriminator loss for the GAN network (y-axis on left), while the orange plot corresponds to the commutation loss (y-axis on right). Figure 11-(b) shows the sum of pairwise distances between the hidden estimates generated by the three sensors, i.e.  $\text{Magnitude}(k) = \sum_{l,m=1}^L (\mathbf{H}^l(k) - \mathbf{H}^m(k))^2$ , where,  $k \in \{1, \dots, d_H\}$ , refers to the feature number in the  $d_H$ -dimensional hidden space. Figure 11-(c) shows the individual classification performance of the sensors. It is observed that

the performance of Seismic and Acoustic Sensors improves as the model is updated, but the performance of the imaging sensor is very low.

Figure 12 shows the optimization losses when the commutation term is added to the objective, i.e. only  $\gamma_1$  is set to zero in Equation 16. This amounts to minimizing of the pairwise commutation loss, hence forcing the hidden space estimates to lie in a common subspace. It is seen that including the commutation cost leads to closer hidden spaces (Figure 12-(b)). The performance of the imaging sensor, however, does not significantly increase.

Figure 13 shows the optimization loss when all the terms in Equation 16 are active. The imaging sensor now starts giving better performance. Since the  $L_{\infty,1}$  norm on the selection matrix allows representation of private/shared features in the hidden space, the heterogeneity of the imaging sensor is maintained, and selected features are more optimal for classification based on the imaging sensor. The effects of the

$L_{\infty,1}$  norm can also be seen in the differences between the hidden estimates in Figure 13-(b), where some features now exhibit more distinguishing diversity compared to others, as they may correspond to private features.

### C. Robustness Analysis

The major advantage of learning a hidden space between the modalities is the ability to detect sensor damage in operation, and to generate representative features for that damaged sensor as seen in Equation 32. The contribution of the representative features towards the fused decision can also be controlled via the degree of confidence.

We also study how the performance of the system varies with different Signal to Noise Ratios. That is noise is selectively added to some sensors while another is normally functioning.

Figures 14 and 15 show the degradation of the fusion performance as the SNR decreases for Dataset-1 and Dataset-2, respectively. The plots with ‘asterisk’(\*) markers represent approaches that search for a common subspace in order to fuse the different modalities, while those with ‘dot’(.) markers represent approaches that perform fusion at the decision level. Finally, the plots with ‘square’ markers show the performance of our proposed approach. The blue plot uses adaptive DoC ( $DoC_t^l = (1 - p_D(\hat{h}_t^l)) \cdot Acc_{train}^l$ ), while the orange plot only uses the prior information ( $DoC_t^l = Acc_{train}^l$ ), which is also the case for other plots using decision level fusion. It is observed that it is important to update the DoC during the implementation based on the sensor condition, rather than only depending on the prior information about the discriminative abilities of the sensor.

Furthermore, the above graphs show that the degradation has severe effects in the case where the seismic and imaging sensors are damaged. This is due to the fact that the discriminative power of the acoustic sensor is low, and in spite of adapting the DoC and generating representative features, the performance is limited by the information contained in the observations of the sensor. A similar trend is also observed for Dataset-2, where the telescopic imagery has lower discriminative ability compared to the radar sensors.

## VI. CONCLUSION

In this work, we proposed a data driven approach that learns a structured hidden space between sensors by the way of a bank of Generative Adversarial Networks. The hidden space is used to learn the features of interest for target classification. The hidden space serves a dual purpose of detecting noisy/damaged sensors and mitigating sensor losses by ensuring a graceful performance degradation. Experiments on multiple datasets show that the proposed approach secures a great degree of robustness to noisy/damaged sensors, and outperforms existing fusion algorithms.

## REFERENCES

- [1] D. L. Hall and J. Llinas, An introduction to multisensor data fusion, Proceedings of the IEEE, vol. 85, no. 1, pp. 623, Jan 1997.
- [2] Bahador Khaleghi, Alaa Khamis, Fakhreddine O. Karray, and Saiedeh N. Razavi, Multisensor data fusion: A review of the state-of-the-art, Information Fusion, vol. 14, no. 1, pp. 28–44, 2013.
- [3] Wang, Han, Erik Skau, Hamid Krim, and Guido Cervone. "Fusing heterogeneous data: A case for remote sensing and social media." IEEE Transactions on Geoscience and Remote Sensing 99 (2018): 1-13.
- [4] Arthur P Dempster, A generalization of bayesian inference., Classic works of the dempster-shafer theory of belief functions, vol. 219, pp. 73104, 2008.
- [5] Glenn Shafer et al., A mathematical theory of evidence, vol. 1, Princeton university press Princeton, 1976.
- [6] Lingjie Li, Data fusion and filtering for target tracking and identification, Ph.D. thesis, 2003.
- [7] Lingjie Li, Zhi-Quan Luo, Kon Max Wong, and Eloi Bosse, Convex optimization approach to identify fusion for multisensor target tracking, IEEE Transactions on Systems, Man, and Cybernetics-Part A: Systems and Humans, vol. 31, no. 3, pp. 172178, 2001.
- [8] Mihai Cristian Florea and Eloi Bosse, Critiques on some combination rules for probability theory based on optimization techniques, in Information Fusion, 2007 10th International Conference on. IEEE, 2007
- [9] Roheda, Siddharth, Hamid Krim, Zhi-Quan Luo, and Tianfu Wu. "Decision Level Fusion: An Event Driven Approach." In 2018 26th European Signal Processing Conference (EUSIPCO), pp. 2598–2602. IEEE, 2018.
- [10] Roheda, S., Krim, H., Luo, Z.Q. and Wu, T., 2019. Event Driven Fusion. arXiv preprint arXiv:1904.11520.
- [11] Judy Hoffman, Saurabh Gupta, and Trevor Darrell, Learning with side information through modality hallucination, in Proceedings of the IEEE Conference on Computer Vision and Pattern Recognition, 2016, pp. 826834.
- [12] Geoffrey Hinton, Oriol Vinyals, and Jeff Dean, Distilling the knowledge in a neural network, arXiv preprint arXiv:1503.02531, 2015.
- [13] Vladimir Vapnik and Rauf Izmailov, Learning using privileged information: similarity control and knowledge transfer., Journal of machine learning research, vol. 16, no. 20232049, pp. 55, 2015.
- [14] Siddharth Roheda, Benjamin S Riggan, Hamid Krim, and Liyi Dai, Cross-modality distillation: A case for conditional generative adversarial networks, in 2018 IEEE International Conference on Acoustics, Speech and Signal Processing (ICASSP). IEEE, 2018, pp. 29262930.
- [15] Sarah Rastegar, Mahdieh Soleymani, Hamid R Rabiee, and Seyed Mohsen Shojaee, Mdl-cw: A multimodal deep learning framework with cross weights, in Proceedings of the IEEE Conference on Computer Vision and Pattern Recognition, 2016, pp. 26012609.
- [16] Raghuraman Gopalan, Ruonan Li, and Rama Chellappa, Domain adaptation for object recognition: An unsupervised approach, in Computer Vision (ICCV), 2011 IEEE International Conference on. IEEE, 2011, pp. 9991006.
- [17] Jingjing Zheng, Ming-Yu Liu, Rama Chellappa, and P Jonathon Phillips, A grassmann manifold-based domain adaptation approach, in Pattern Recognition (ICPR), 2012 21st International Conference on. IEEE, 2012, pp. 20952099.
- [18] Jie Ni, Qiang Qiu, and Rama Chellappa, Subspace interpolation via dictionary learning for unsupervised domain adaptation, in Proceedings of the IEEE Conference on Computer Vision and Pattern Recognition, 2013, pp. 692699.
- [19] Ian Goodfellow, Jean Pouget-Abadie, Mehdi Mirza, Bing Xu, David Warde-Farley, Sherjil Ozair, Aaron Courville, and Yoshua Bengio, Generative adversarial nets, in Advances in neural information processing systems, 2014, pp. 26722680.
- [20] Mehdi Mirza and Simon Osindero, Conditional generative adversarial nets, arXiv preprint arXiv:1411.1784, 2014.
- [21] Jon Gauthier, Conditional generative adversarial nets for convolutional face generation, Class Project for Stanford CS231N: Convolutional Neural Networks for Visual Recognition, Winter semester, vol. 2014, no. 5, pp. 2, 2014.
- [22] Scott Reed, Zeynep Akata, Xincheng Yan, Lajanugen Logeswaran, Bernt Schiele, and Honglak Lee, Generative adversarial text to image synthesis, arXiv preprint arXiv:1605.05396, 2016.
- [23] Phillip Isola, Jun-Yan Zhu, Tinghui Zhou, and Alexei A Efros, Image-to-image translation with conditional adversarial networks, arXiv preprint arXiv:1611.07004, 2016.
- [24] Frobenius, Georg. "Ueber lineare Substitutionen und bilineare Formen." Journal fr die reine und angewandte Mathematik 84 (1877): 1-63.
- [25] Gherardo, Paolo. On common eigenbases of commuting operators.
- [26] Sylvester M Nabritt, Thyagaraju Damarla, and Gary Chatters, Personnel and vehicle data collection at aberdeen proving ground (apg) and its distribution for research, Tech. Rep., ARMY RESEARCH LAB ADELPHI MD SENSORS AND ELECTRON DEVICES DIRECTORATE, 2015.
- [27] Kyunghun Lee, Benjamin S Riggan, and Shuvra S Bhattacharyya, An accumulative fusion architecture for discriminating people and vehicles using acoustic and seismic signals, in Acoustics, Speech and Signal Processing (ICASSP), 2017 IEEE International Conference on IEEE, 2017, pp. 29762980.
- [28] Iyengar, Satish G., Pramod K. Varshney, and Thyagaraju Damarla. "On the detection of footsteps based on acoustic and seismic sensing." In 2007 Conference Record of the Forty-First Asilomar Conference on Signals, Systems and Computers, pp. 2248-2252. IEEE, 2007.
- [29] Bahrampour, Soheil, Nasser M. Nasrabadi, Asok Ray, and William Kenneth Jenkins. "Multimodal task-driven dictionary learning for image classification." IEEE transactions on Image Processing 25, no. 1 (2016): 24-38.
- [30] Christian Szegedy, Vincent Vanhoucke, Sergey Ioffe, Jon Shlens, and Zbigniew Wojna, Rethinking the inception architecture for computer vision, in Proceedings of the IEEE Conference on Computer Vision and Pattern Recognition, 2016, pp. 28182826.
- [31] Peng, Yuxin, and Jinwei Qi. "Cm-gans: Cross-modal generative adversarial networks for common representation learning." ACM Transactions on Multimedia Computing, Communications, and Applications (TOMM) 15.1 (2019): 22.
- [32] Arjovsky, Martin, Soumith Chintala, and Ilya Sutskever. "Wasserstein gan." arXiv preprint arXiv:1701.07875 (2017).